

ATLAS electromagnetic calorimetry and performance of electron/photon detection

Ph. Schwemling
On behalf of the ATLAS Collaboration¹

LPNHE
Universités Paris-6 et Paris-7, IN2P3-CNRS
4, place Jussieu 75252 PARIS CEDEX 05
e-mail: schwemli@lpnhep.in2p3.fr

Received:

Abstract. The design constraints and the target physics performance of the ATLAS Electromagnetic Calorimeter are reviewed, and the construction status is summarized. Test-beam data, covering a large part of the final detector, have been analysed and measurements of several important detector performance estimators are presented. Finally, some aspects of the electron and photon reconstruction and the expected performance of the detector are reviewed.

PACS: not given

1 Introduction

The Liquid Argon Electromagnetic Calorimeter is a crucial tool in the understanding of many physics processes that will be studied by ATLAS with the LHC data. For all physics processes where electron identification, photon reconstruction, jet and missing energy measurement are needed, precise and hermetic calorimetry is of utmost importance at LHC. $H \rightarrow 4e$, $H \rightarrow WW$, and the W mass measurement particularly gain from excellent calorimetric performance. Dynamic range, resolution and uniformity are the main parameters that have to be optimized to reach this goal.

As has been determined from physics simulation [1], the calorimeter has to obey to the following constraints :

- The hermeticity should be as perfect as possible, and the design should avoid uninstrumented areas (“cracks”).
- For Higgs boson decays to two photons or to four electrons, in the mass range going from 90 to 180 GeV/ c^2 , the calorimeter should allow a resolution of 1% on the Higgs mass measurement. This translates into a sampling term of $10\%/\sqrt{E}$ or better, and a constant term better than 1%. The total depth of the calorimeter has to be at least $24 X_0$, to minimize the effect of longitudinal leakage on the energy resolution above 500 GeV/ c^2 .

- The dynamic range has to cover 30 MeV up to 1 TeV, i.e. from the typical noise level up to the single cell energy expected in the case of the decay of a Z' or W' boson with a mass of 5 to 6 TeV.
- The detector has to be able to identify electrons with transverse momenta as low as 1-2 GeV/ c up to a few TeV/ c . The rejection factor against jets should be of the order of 10^5 to select electrons exclusively, as a starting point for analyses using high p_T leptons. To observe the $H \rightarrow \gamma\gamma$ decay, a rejection factor of 3000 is needed to sufficiently suppress the γ -jet and jet-jet backgrounds. The ability of the calorimeter to distinguish to some extent between π^0 related energy deposits and photons is essential to achieve this goal.
- In addition to all these requirements, the harsh radiation conditions at LHC speak for a technology whose stability with time can be easily maintained, and that has good tolerance to irradiation.

2 Detector Design

To address the above requirements, ATLAS has chosen to build a Lead/Liquid Argon Electromagnetic Calorimeter, comprising a barrel and two end-cap parts. The barrel calorimeter, covering the $|\eta|$ range from 0 to 1.475, shares its cryostat with the superconducting solenoid, the calorimeter being behind the solenoid. Both end-caps are in the same cryostats as the hadronic and forward Liquid Argon Calorimeters. Since the material in front of the calorimeters amounts to about $1.5 X_0$ on average, up to $2 X_0$ at the barrel to end-cap transition, both the End-Cap and Barrel Calorimeter are complemented with presampler detectors that cover up to $|\eta| = 1.8$. Their purpose is to evaluate the amount of energy loss in the material in front of the calorimeter. Basically, these presamplers are thin layers of argon equipped with readout electrodes but no absorber.

A general view of the mechanical structure of the Barrel Electromagnetic Calorimeter is given in figure 1. The peculiar shape of the accordion has been chosen for the absorbers and electrodes because it allows one to build the detector without any cracks in ϕ , with the HV supply cables and signal cables only running on the front and back face of the detector. These cables pass through the feedthroughs situated at the extremities of the cryostat, and are connected to the Front-End boards located in the crates sitting above the feedthroughs. Furthermore, the accordion structure can be fine-tuned to give a very small ϕ response modulation (at the level of a few per mille). By reducing the length of the path needed to connect the readout cell to the readout electronics, the accordion structure also allows one to minimize the inductance in the signal path, so that it is possible to use a fast shaping circuit to cope with the 25 ns bunch crossing time of the LHC.

The End-Cap Calorimeter, covering the $|\eta|$ range from 1.4 to 3.2, has a mechanical structure similar to the Barrel Calorimeter, but with absorbers arranged like the spokes of a bicycle wheel, as can be seen from figure 2. However, whereas the Barrel Calorimeter uses only one type of absorber (using two lead

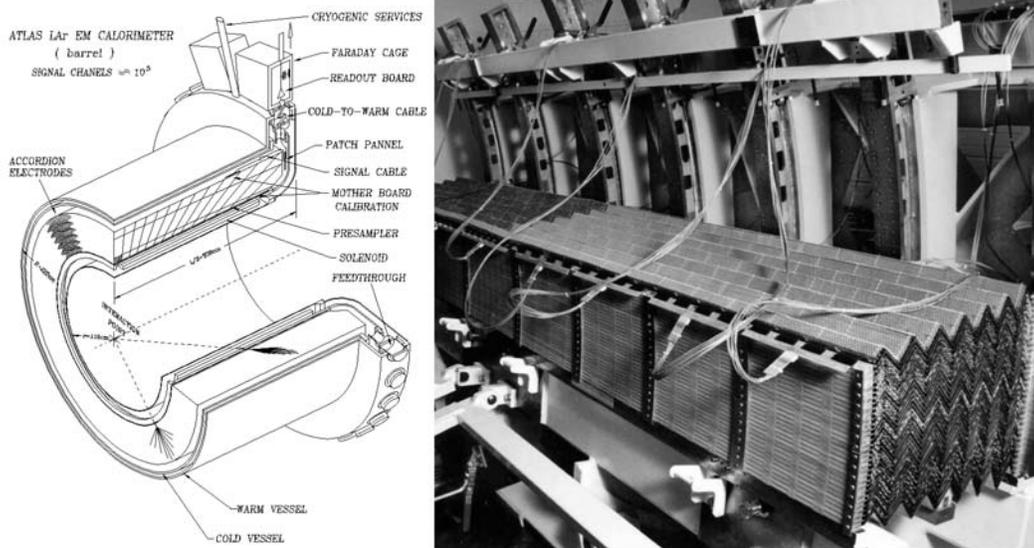


Fig. 1. Left : general view of one half of the Electromagnetic Barrel Calorimeter inside of its cryostat. The length of the half Barrel is about 3.5 m and its diameter 4.5 m. Right : photograph of a module during construction.

thicknesses) and has a gap thickness constant over the whole detector, the End-Cap Calorimeter has a varying gap thickness as a function of $|\eta|$ and uses two different types of absorbers, one for the outer wheel ($1.4 < |\eta| < 2.5$), and one different type for the inner wheel ($2.5 < |\eta| < 3.2$). The varying gap thickness requires different HV values as a function of η regions to maintain a constant response with η . The structure and the understanding of the End-Cap Calorimeter is therefore more complex than in the case of the barrel structure.

The Barrel Calorimeter η range is covered by two readout electrodes, the first one extending from $|\eta| = 0$ to $|\eta| = 0.8$, and the second one covering the range $|\eta| = 0.8$ to $|\eta| = 1.4$. The transition between the electrodes also corresponds to a change in lead thickness, needed to prevent the sampling ratio (and consequently, the sampling term) of the calorimeter from increasing too much at high η . The End-Cap Calorimeter also has two types of electrodes, the first one covering the $|\eta|$ region from 1.4 to 2.5, and the second one from 2.5 to 3.2. Similarly to the barrel, the transition between the two electrodes also corresponds to a transition between lead thickness within the absorbers. The ATLAS Tracker covers up to $|\eta| = 2.5$, which is the η region that will be used for “precision physics”, combining tracking and calorimeter information, requiring the calorimeter to be fine-grained to ensure efficient calorimeter-tracker association. Above $|\eta| = 2.5$, the calorimeter granularity is coarser.

The first sampling section of the calorimeter has a very fine granularity ($\Delta\eta \times \Delta\phi = 0.003 \times 0.1$), to optimize the ability to separate photons from π^0 energy deposits, and electrons from jets. The second sampling section, mainly devoted to energy measurement, has a granularity of 0.025×0.025 , and the back sampling

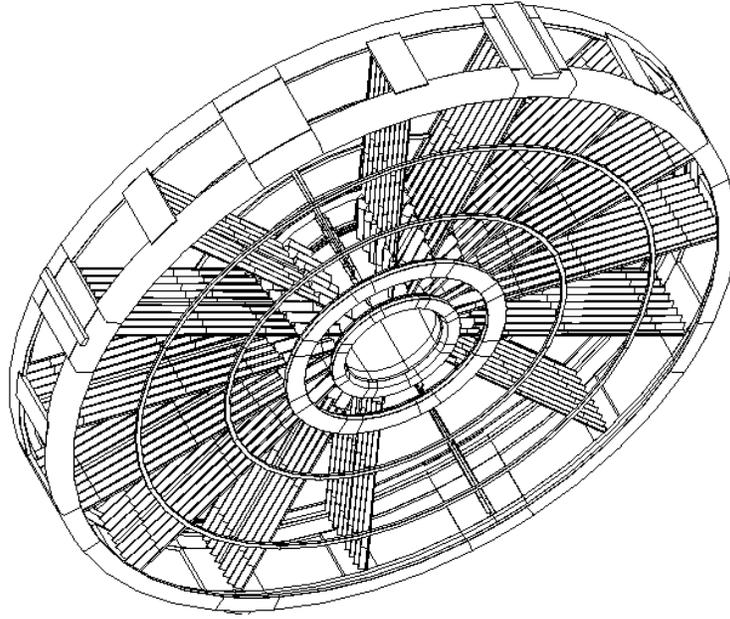


Fig. 2. General view of one wheel of the Electromagnetic End-Cap Calorimeter. The diameter is about 4.5 m, and the thickness is about 1 m.

has a slightly coarser granularity, $\Delta\eta \times \Delta\phi = 0.050 \times 0.025$.

More technical details on the End-Cap and Barrel Electromagnetic Calorimeter can be found in [2].

3 Status of the Construction

3.1 Barrel Calorimeter

The stacking of all the Barrel Calorimeter modules (in total 32 modules of 63 absorbers and 128 electrodes each) was finished by the end of April 2003. All in all, the construction of these series modules has taken about three years, including procurement, production of absorbers and electrodes as well as the stacking itself. Since quality control measurements are now available for all parts of the calorimeter, it is possible to get a first perception of the performance that will be reached by the completed detector. For example, from the lead and absorber quality control measurements, it is possible to estimate that the contribution to the total constant term coming from the mechanical structure of the calorimeter will be slightly below 0.3%, as was hoped for at the time of design of the detector.

All 32 modules have been successfully assembled into two cylindrical separate half-barrels. One of these has already been inserted into the cryostat, including its presampler (see figure 3). After insertion, extensive electrical tests have been performed. In total, only about 10 channels out of about 50000 have been found

non-working. The second wheel is presently being prepared for its insertion into the cryostat, which should take place September 2003.

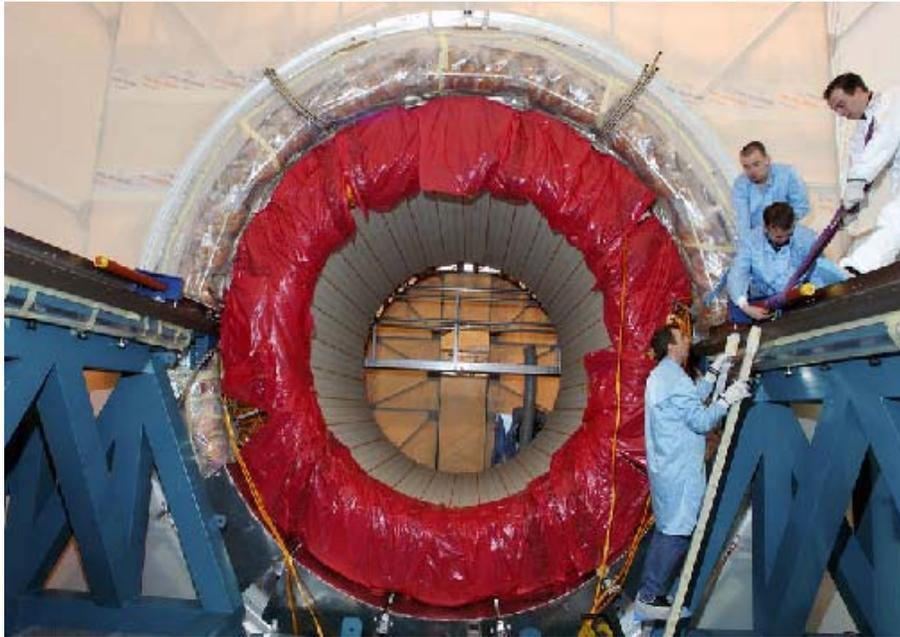


Fig. 3. Photograph of the first Barrel Calorimeter wheel, including the Presampler, after insertion into the cryostat.

3.2 End-Cap Calorimeter

The stacking of end-cap modules is still in progress; presently there are 11 modules ready for assembly, out of a total of 16. The module stacking should be completed by February 2004. One complete end-cap wheel (inner and outer wheel) comprises in total 8 modules, one of which has already been assembled (see figure 4).

4 Detector Performance

Four Barrel and three End-Cap Calorimeter modules have been tested between 2000 and 2002. The analysis of the data is still ongoing. However, the already established results allow one to have a good conception of the quality of the detector. Among the various topics studied, there are now well established results on energy resolution, module uniformity, position resolution, crosstalk, response to minimizing ionizing particles (MIP) and timing resolution.

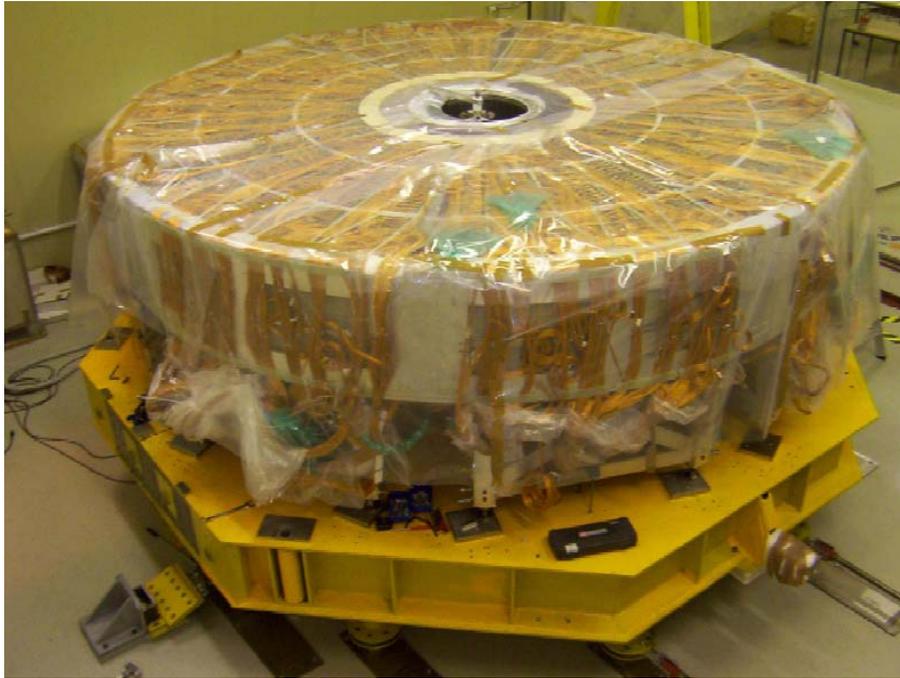


Fig. 4. Photograph of the first End-cap Calorimeter wheel, after assembly.

4.1 Test-Beam Setup

The barrel and end-cap setups are very similar. They are both located at CERN, in the North Area. In both cases, the test-beam setup comprises of a rotating table supporting the cryostat with the module inside, to allow for position scans. Four beam chambers, placed in front of the cryostat, are used to compute event by event the impact point on the detector. Four plastic scintillators associated with fast photomultipliers provide a fast trigger signal. In addition, a scintillator behind a $3 X_0$ lead absorber (“pion counter”), placed behind the cryostat allows one to tag pions contaminating the beam. Similarly, a scintillator behind 5λ of Iron (“muon counter”) placed further downstream, allows one to tag muons.

Most tests have been done with electrons in the 10 - 300 GeV energy range particularly for position scans uniformity. The readout electronics is similar to the final ATLAS electronics, since it is made of boards fonctionnally identical to the final ones, which, however, do not yet use radiation resistant ASICs. A detailed description of the test-beam setups, module construction and performance evaluation can be found in [4] and [5]. However, the modules studied in [4] and [5] were pre-production modules (“Module 0”), whereas the results presented hereafter have been obtained on series modules.

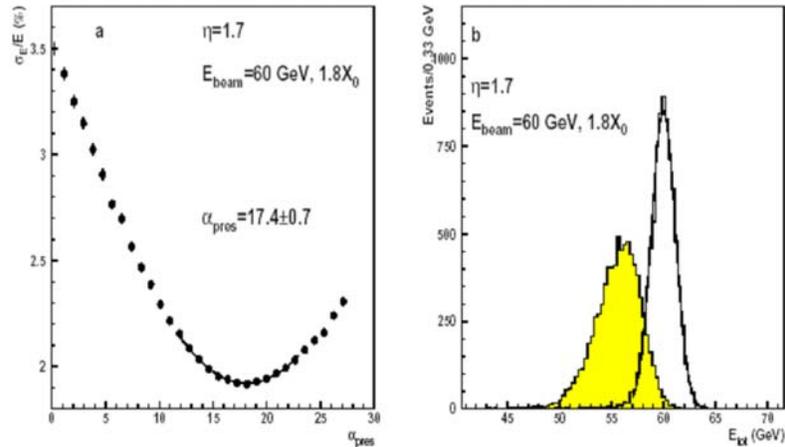


Fig. 5. Optimisation of the presampler weight for testbeam data, with $1.8 X_0$ dead material (lead) in front, for a 60 GeV electron beam. Left : energy resolution as a function of presampler weight. Right : Energy distribution without weighting (shaded histogram), and with optimal presampler weight (open histogram). The gain in resolution is obvious.

4.2 Signal Reconstruction

Energy and time measurement are based on a method called “optimal filtering”. The basic principle is to use as energy and time estimators linear combinations of several time consecutive samples taken on the signal pulse. The coefficients of the linear combinations are computed to minimize the noise of the energy measurement. Practically, to compute the coefficients, one needs to know the noise auto-correlation matrix that can be obtained from pedestal runs, and also the signal shape and its first derivative. The reconstruction of the signal shape has proven to be quite tricky although manageable in the end. To reconstruct the physics signal shape, the first step is to accurately reconstruct the shape of the calibration signal. Next, one has to take into account the difference of shape between the injected signal, since the physics signal is triangular, whereas the calibration signal is a decaying exponential. In addition, calibration and physics signal are not injected at the same point in the electronics chain, as the calibration current is injected at the motherboard and summing board level. One therefore has to carefully model the part of the signal path that is different between calibration and physics effect.

Once the optimal filtering coefficients have been computed for each cell, it is possible to get raw energy measurements cell by cell. Next one has to search for the optimal weight for the presampler correction. Figure 5 shows an example of the procedure. Finally the cluster energy measurements still have to be corrected for ϕ modulation, and for lateral shower containment effects (see figure 6).

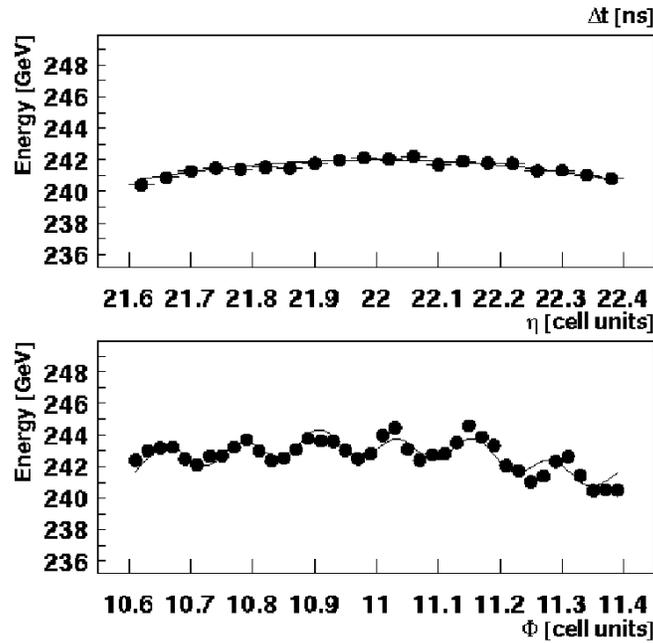


Fig. 6. Above : Reconstructed energy as a function of η . Below : ϕ modulation.

4.3 Some Selected Test-Beam Results

4.3.1 Energy Resolution: Energy resolution as a function of electron energy is one of the first parameters of the detectors that has been checked in the test-beam. For both Barrel and End-Cap Calorimeters, it has been found that the results were satisfactory and in good agreement with the simulation. For example, at $\eta = 0.3625$, in the barrel, the measured sampling term is 9.24%, with a local constant term of 0.23%. In the end-cap, at $\eta = 1.9$, we have obtained a sampling term of 10.35% and a local constant term of 0.27%.

4.3.2 Uniformity: For most of the barrel (515 cells), the uniformity is 0.57%. The uniformity is estimated as the r.m.s of the distribution of the calorimeter response cell by cell. The region around $\eta = 0.8$ (see figure 7), corresponding to the transition between the two types of barrel electrodes and also to the transition between the two barrel lead thicknesses, is still being worked on. In the case of the end-cap, the uniformity on regions of a size of 0.2×0.4 in $\eta \times \phi$ is of the order of 0.4%-0.6%. On one complete module, we obtain an uniformity of 0.6% (see figure 8).

4.3.3 Position and Angular Resolution: A good shower position resolution is useful in the search for $H \rightarrow \gamma\gamma$ decays. This has been studied both in the barrel and end-caps. For the barrel we have found a position resolution of $\sigma(\eta) = 0.09 \times 10^{-4} \oplus 0.12 \times 10^{-2} \text{GeV}^{-1}/E$ in the first sampling, and of

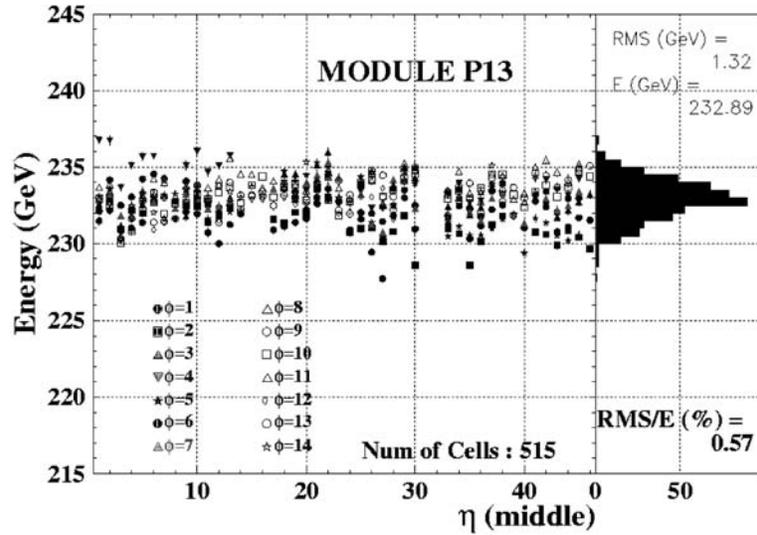


Fig. 7. Uniformity of energy measurements in one barrel module, for a 235 GeV electron beam. Each dot corresponds to one cell.

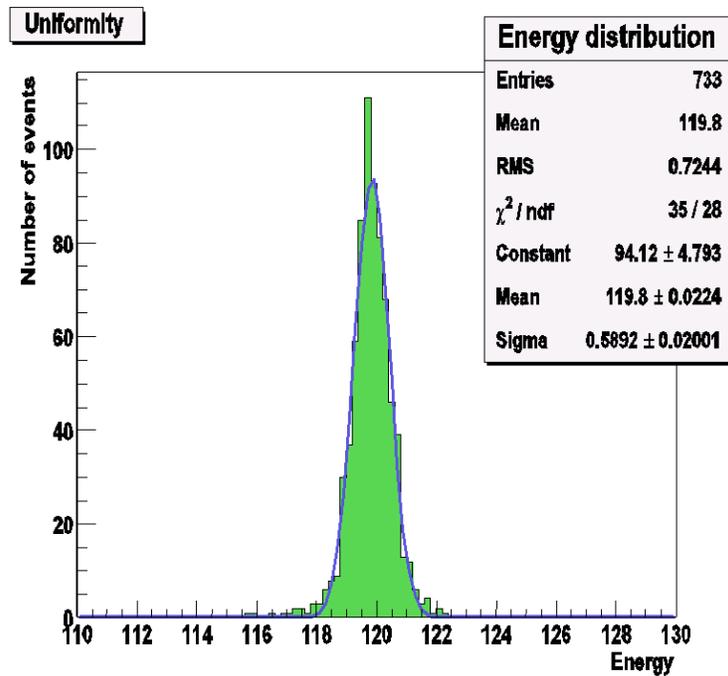


Fig. 8. Uniformity of energy measurements in one end-cap module, for a 120 GeV electron beam.

$0.04 \times 10^{-4} \oplus 0.46 \times 10^{-2} \text{ GeV}^{-1/2}/\sqrt{E} \oplus 0.23 \times 10^{-2} \text{ GeV}^{-1}/E$ in the middle sampling. In the case of the end-cap, the angular resolution in radians, as a function of beam energy, has been measured to be $\sigma_\theta = 0.048 \sqrt{E_{beam}} \oplus 0.095/E$, with the energies given in GeV.

4.3.4 Calorimeter Response to MIP: Using the fact that some muons were always contaminating the electron beam, we have investigated the response to muons crossing the calorimeter. We have found that it was possible to extract a very clean muon signal above the pedestal, with a signal over noise ratio of about 7. However, the signal over noise ratio will go down to about 5 at LHC, due to a different shaping time constant at LHC, compared to the test beam.

4.3.5 $\gamma - \pi^0$ Separation: In the search for $H \rightarrow \gamma\gamma$ decays, the calorimeter has to provide a rejection of about 3 for a photon identification efficiency of 90%, using the fine granularity in the first sampling. This has been checked on specific test-beam data, obtained by inserting some material in the beam line upstream of a bending magnet, to cause the incoming electron to emit hard bremsstrahlung photons. By selecting events with the appropriate kinematics, it was possible to mimick a π^0 decay to two photons. The agreement between simulation and data is satisfactory, and it could be shown that the required rejection factor is reached.

4.3.6 Time Resolution: The ATLAS Electromagnetic Calorimeter not only provides energy measurements, but it has also the capability to measure the time of the impact of particles. This capability can be used at the startup of LHC, to understand and reject instrumental backgrounds like beam-gas events. It will also be useful to search for the decay $\chi^0 \rightarrow \tilde{G}\gamma$ occurring in GMSB SUSY models, making use of the fact that the χ^0 is long-lived and so the photon is emitted with some delay with respect to the beam crossing. By comparing the timing measurements from two cells within the same electromagnetic cluster, it has been estimated that the time resolution of the calorimeter is better than 100 ps for energies above 30 GeV/c².

4.3.7 Crosstalk Measurements: The crosstalk has been measured using calibration pulse runs. In all cases that have been studied, the crosstalk is below 0.5%. The only exception is the strip to strip crosstalk in the first sampling section that is dominated by capacitive edge effects, giving a crosstalk value of 4%.

5 Some Electron and Photon Reconstruction Issues

In this section, we will summarize the strategies that have been studied to identify electrons and photons coming from various physics processes. In particular, we will show how the interplay between Inner Detector and calorimeter can in many cases improve the reconstruction with respect to the possibilities of each detector used standalone. More details can be found in [3].

5.1 Bremsstrahlung Photons

An important issue in the electron reconstruction with the calorimeter is to take into account the effects of bremsstrahlung. Indeed, the Inner Detector represents 0.5 to 1.2 X_0 of matter (depending upon η) in front of the calorimeter, so that the probability of significant energy loss can be quite significant : Typically, every 5th electron loses 50% or more of its energy while crossing the Inner Detector. This translates into significant tails in the ratio of true to reconstructed p_T for electrons (see figure 9). Two strategies have been evaluated to take into account this effect :

- Taking into account the bremsstrahlung at the track fitting level by incorporating the corresponding energy loss in the Kalman filter as an additional term. This procedure increases the reconstruction efficiency by 6% with respect to the standard fit of figure 9, but the p_T resolution is worsened by a factor of 2, see figure 9.
- For a single hard radiation, the energy-weighted barycenter of the impact point of the electron and bremsstrahlung photon lies on the track of the initial electron. This means that it is possible to measure the momentum of the electrons by fitting the track segment before the radiation took place, plus the position within the calorimeter. In this case, the efficiency is increased by 2%, and the p_T resolution is no longer degraded.

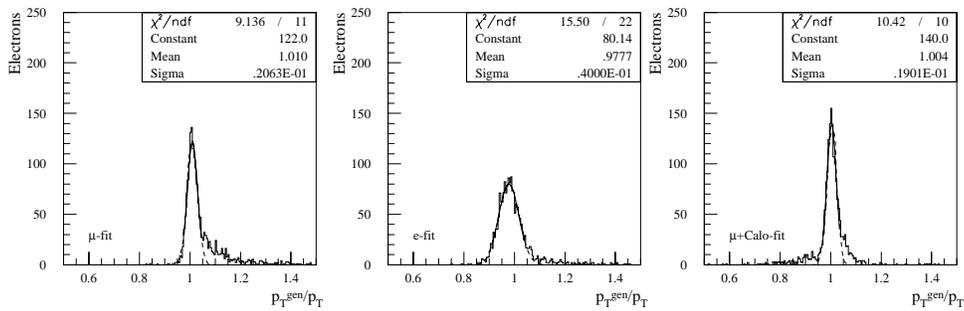


Fig. 9. All plots show the distribution of true over reconstructed p_T , for 20 GeV/c electrons at $\eta = 0.3$. Left, track fit without taking bremsstrahlung into account. Middle, bremsstrahlung has been taken into account into the track fit. Right, calorimeter position measurement included in the track fit.

5.2 E/p Measurement, Calibration

The main tool for calibration of the calorimeter, however, will be the decays $Z \rightarrow ee$. At low luminosity, the rate of such events is expected to be about 1 Hz, so that within few days it should be possible to calibrate 400 regions of the calorimeter to 0.3%.

The E/p measurements are very useful for electron identification and can also be used to cross-check the detector calibration. The knowledge of the E/p

resolution allows to easily estimate the number of events needed to check the calibration of the calorimeters, assuming that the momentum scale is known from the Inner Detector. The resolution that can be achieved is of the order of 5%, independent of η . With such a resolution on E/p , it is possible to calibrate 400 regions in the calorimeter with a statistical precision of 0.1%, using 10^6 electrons. This will probably not be difficult, since one expects to collect 30 million of $W \rightarrow e\nu$ decays within one year of running at low luminosity.

5.3 Low Energy Electrons

The efficient tagging of low energy electrons is an important tool for B-physics. Separating low energy electrons from pions by analysing the energy deposits in the calorimeter alone is not an easy task, since these electrons are within or near to jets. A better option in this case is to start from the Inner Detector tracks and to analyse the energy deposits around their extrapolated position in the calorimeter. By combining various shower shape estimators, the E/p value and the information from the Transition Radiation Tracker, it is possible to get the pion rejection versus electron efficiency curves of figure 10.

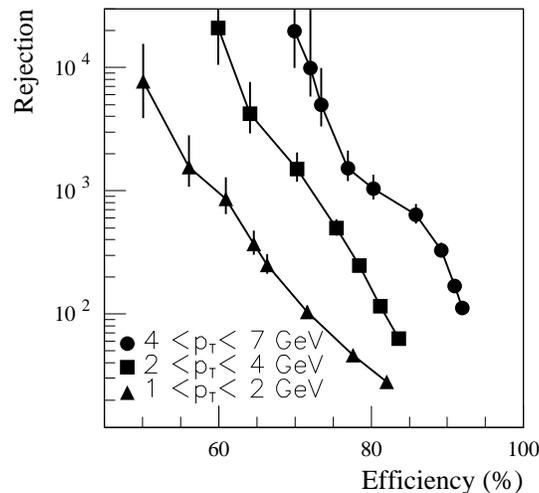


Fig. 10. Pion rejection factor versus soft electron tagging efficiency, for various p_T ranges.

5.4 Electron/Jet And Photon/Jet Separation

Identification of isolated electrons of high p_T (> 20 GeV/ c) is essential to LHC physics. To obtain an inclusive electron signal, a rejection against jets of the order of 10^5 is mandatory. Extensive simulations have shown that by combining shower shape estimators (including energy deposits in the Hadronic Calorimeter) and requiring a good energy-momentum and position match, it is possible to obtain a 10^5 rejection factor for a p_T of 30 GeV/ c , with an electron identification efficiency

of 70%, at low luminosity. At high luminosity, the corresponding rejection factor is 45000.

Given the amount of material in front of the calorimeter, many of the photons are converted. Since the $H \rightarrow \gamma\gamma$ signal is small, it is important to recover the conversions to maintain its efficiency as high as possible. Conversions are first searched for in the Inner Detector, and the energy deposited in the calorimeter in a $3 \times 7 \eta \times \phi$ window is computed, since this window size allows one to recover a significant fraction of the initial photon energy. Using an estimated dependance between the conversion radius, E_T and the photon energy, it is possible to reconstruct the initial photon energy.

If the photon has not been reconstructed as a conversion, the separation relies mainly on a shower shape analysis in the calorimeter, and on the requirement that no track be found in the inner detector within a $\Delta\eta \times \Delta\phi$ region of size $\pm 0.1 \times \pm 0.1$ around the calorimeter cluster. The jet rejection obtained is of the order of 3000 above $E_T \simeq 30$ GeV.

5.5 Mass Reconstruction

Using all tools described above, including conversion reconstruction in the case of photons, it has been estimated that the Higgs mass resolution, for a Higgs of $130 \text{ GeV}/c^2$, is $1.3 \text{ GeV}/c^2$ at low luminosity. The acceptance is 80% within 1.4σ of the mean value. At high luminosity, for the same acceptance, the resolution worsens to $1.55 \text{ GeV}/c^2$.

In the case of the $H \rightarrow 4e$ decay, again for a Higgs mass of $130 \text{ GeV}/c^2$, the resolution at low luminosity is $1.54 \text{ GeV}/c^2$, for an acceptance of 84% within $\pm 2\sigma$ of the mean value. At high luminosity, the resolution worsens to $1.81 \text{ GeV}/c^2$, for the same acceptance value.

6 Conclusions

Significant parts of the calorimeter have now been manufactured, tested and assembled, and several important and sometimes difficult milestones have been passed, like insertion of the first barrel wheel and assembly of the first end-cap wheel. The next major steps forward are the full test of a complete ATLAS readout electronics crate by the end of 2003 and the filling of the cryostats with Liquid Argon, which is planned for 2004.

A lot of effort has been put into the test-beam data taking and in the subsequent analyses of the data. The results give us confidence that the final detector will meet the very demanding specifications for an LHC detector. The next steps are combined test-beams measurements that will be take place in 2004, including the Inner Detector, the Electromagnetic and Hadronic Calorimeters. These will give us the possibility to optimize the online software, understand and tune the simulation of hadronic showers in ATLAS, understand the energy scale of the detector, and finally to test and prepare the calibration and detector intercalibration procedure. This thorough preparation is a prerequisite for the delivery of quality physics data that will permit data analyses as rapidly as possible after start-up of the LHC.

References

1. The ATLAS collaboration, ATLAS Calorimeter Performance Technical Design Report, CERN/LHCC/96-40.
2. The ATLAS collaboration, ATLAS Liquid Argon Calorimeter Technical Design Report, CERN/LHCC/96-41.
3. The ATLAS collaboration, ATLAS Detector and Physics Performance Technical Design Report, CERN/LHCC/99-14.
4. The ATLAS Electromagnetic Liquid Argon Calorimeter Group (B. Aubert et al), "Performance of the ATLAS Electromagnetic Calorimeter Barrel Module 0", Nuclear Instruments and Methods A 500 (2003), 202-231.
5. The ATLAS Electromagnetic Liquid Argon Calorimeter Group (B. Aubert et al), "Performance of the ATLAS electromagnetic calorimeter End-cap Module 0", Nuclear Instruments and Methods A 500 (2003), 178-201.